Polarization-gradient-assisted subrecoil cooling: Quantum calculations in one dimension

P. Marte, R. Dum, R. Taïeb, and P. Zoller
Joint Institute for Laboratory Astrophysics and Department of Physics, University of Colorado, Boulder, Colorado 80309-0440

M. S. Shahriar
Research Laboratory of Electronics, Massachusetts Institute of Technology, Cambridge, Massachusetts 02139

M. Prentiss
Harvard University Lyman Laboratory of Physics, Cambridge, Massachusetts 02138
(Received 3 December 1993)

We present a fully quantum-mechanical analysis of laser cooling of an angular momentum $J_g = 1$ to $J_e = 1$ transition in a laser configuration consisting of two counterpropagating linearly polarized laser beams. The essential feature of this configuration is the coexistence of velocity-selective coherent population trapping (VSCPT) and polarization-gradient cooling. The role of polarization-gradient cooling is to provide (i) for short interaction times "precooling" of the initial momentum distribution and (ii) in the long-time limit "confinement of velocities." This eventually leads to a larger number of atoms being captured in the dark state when compared with the scheme of Aspect *et al.* [Phys. Rev. Lett. **61**, 826 (1988)]. We find that the optimum parameter values for polarization-gradient cooling and VSCPT are in a completely different parameter regime: polarization-gradient cooling works best off resonance and for low intensities, while VSCPT works best on resonance. We can combine the advantages of polarization-gradient cooling and VSCPT in a scheme where we cycle in time between the optimum cooling parameters for both cooling mechanisms.

PACS number(s): 32.80.Pj, 42.50.Ar

I. INTRODUCTION

Kinetic energies achieved in laser Doppler cooling of two-level atoms are of the order $E = \hbar\Gamma/2$, with Γ the spontaneous decay rate of the excited state of the atom. Polarization-gradient cooling of atoms with Zeeman substructure by a Sisyphus cooling typically leads to energies of the order of a few tens of recoil energies E_R [1], where the one-photon recoil energy is defined as $E_R = \hbar^2k^2/2M$, with $k = 2\pi/\lambda$ the wave number of the atomic transition and M the mass of the atom. For heavy atoms and dipole-allowed transitions, $E_R \ll \hbar\Gamma$ and temperatures achieved in polarization gradient cooling are much lower than for Doppler cooling. Energies below the recoil limit $E < E_R$, corresponding to an atomic de Broglie wavelength longer than the wavelength of the light λ, can be obtained by optical pumping into a velocity-selective dark state [2]. This can be realized by velocity-selective coherent population trapping (VSCPT) in a three-level Λ system [3,4] or by cooling with a sequence of shaped Raman pulses where the frequency spectrum of the light is tailored so that atoms with near-zero velocity are no longer excited [5]. While dark-state cooling produces subrecoil temperatures, these mechanisms are based on a random walk (diffusion) in momentum space and thus—in particular in two-dimensional (2D) and 3D configurations [2,6,7]—have efficiencies significantly lower and cooling times much longer than Doppler and polarization-gradient cooling.

In their work on VSCPT, Aspect *et al.* [3] considered a 1D laser configuration with counterpropagating σ_+ and σ_- polarized lasers. In this configuration the positive frequency part of the electric field propagating along the z axis has the form

$$\vec{E}^{(+)}(z,t) = \mathcal{E}(e^{+ikz}\vec{e}_{+1} + e^{-ikz}\vec{e}_{-1})e^{-i\omega t}, \tag{1}$$

with $\vec{e}_{\pm1} = \mp(\vec{e}_x \pm i\vec{e}_y)/\sqrt{2}$ spherical unit vectors. For a $J_g = 1$ to $J_e = 1$ transition, as for metastable He $2s\ ^3S_1$–$2p\ ^3P_1$, the two ground-state superpositions

$$\langle z \mid \psi_{NC,C}(p) \rangle = e^{+ipz/\hbar}|g_{-1}\rangle \pm e^{-ipz/\hbar}|g_{+1}\rangle \tag{2}$$

correspond to a noncoupled (coupled) state. In particular the atom has a velocity-selective dark state

$$\langle z \mid D \rangle \equiv \langle z \mid \psi_{NC}(0) \rangle = e^{+ikz}|g_{-1}\rangle + e^{-ikz}|g_{+1}\rangle\ . \tag{3}$$

We denote the ground and excited states by $|g_m\rangle$ and $|e_m\rangle$, respectively, with $m = -1, 0, +1$ Zeeman quantum numbers. In this running-wave (RW) case, induced emission processes couple only states within a momentum family $\mathcal{F}(p) = \{|p - \hbar k, g_{-1}\rangle, |p, e_0\rangle, |p + \hbar k, g_{+1}\rangle\}$ while emission of a spontaneous photon with projection of the photon momentum $-\hbar k \le \hbar u \le \hbar k$ along the z axis corresponds to a quantum jump $\mathcal{F}(p) \to \mathcal{F}(p + \hbar u)$ [8]. If in this random walk in momentum space the dark state (1) in the momentum family $\mathcal{F}(p = 0)$ is populated by a quantum jump, the atom will remain trapped in this

 ©1994 The American Physical Society

state while a noncoupled state with momentum close to zero will have a decay rate back to the coupled state proportional to $(kp/m)^2$. Thus, as a function of time an increasing number of atoms within the excitation profile of the laser will accumulate in noncoupled states close the dark state (3).

In this paper we present results of an analysis of VSCPT in a σ_+-σ_- *standing-wave* (SW) configuration for a $J_g = 1$ to $J_e = 1$ transition (Fig. 1). The laser configuration consists of two counterpropagating linearly polarized light waves where the angle between the polarization vectors is denoted by θ,

$$\vec{E}^{(+)}(z,t) = \mathcal{E}/\sqrt{2}[\cos(kz+\theta/2)\,\vec{e}_{+1} + \cos(kz-\theta/2)\,\vec{e}_{-1}]e^{-i\omega t}\,. \quad (4)$$

The essential feature of this model is the *coexistence of polarization-gradient cooling and VSCPT* where polarization-gradient cooling provides a precooling mechanism which is expected to lead to an enhanced pumping rate into the dark state. This dark state has the form

$$\langle z \mid D \rangle = \cos(kz-\theta/2)|g_{+1}\rangle + \cos(kz+\theta/2)|g_{-1}\rangle \quad (5)$$

and shows again a double-peaked momentum distribution at $p = \pm\hbar k$. A semiclassical analysis of the cooling force has been given by Shahriar and co-workers [9,10] and optimum cooling was found for an angle of $\theta = \pi/4$. From a quantum-mechanical point of view the picture of cooling is best discussed in terms of adiabatic optical potentials: neglecting nonadiabatic mixing and for weak laser excitation the two adiabatic optical potentials obtained by diagonalizing the coupling between the two ground states $|g_{-1}\rangle$ and $|g_{+1}\rangle$ are

$$V^0_{ad}(z) = 0\,, \quad (6)$$

$$V^1_{ad}(z) = U_0[\cos^2(kz-\theta/2) + \cos^2(kz+\theta/2)]\,. \quad (7)$$

In Eq. (6) $U_0 = \Delta s$ is the height of the potential with Δ the laser detuning and $s \ll 1$ the saturation parameter. The existence of a dark state is reflected in the flat adiabatic potential $V^0_{ad}(z) = 0$, while the spatial modulation of $V^1_{ad}(z)$ provides hills for a Sisyphus cooling mechanism. Nonadiabatic transitions couple the motion on the two potentials. Cooling is found for blue detunings $\Delta > 0$ where $V^1_{ad} > V^0_{ad} = 0$ [9]. There is no polarization-gradient cooling for $\Delta = 0$ or $\theta = \pi/2$.

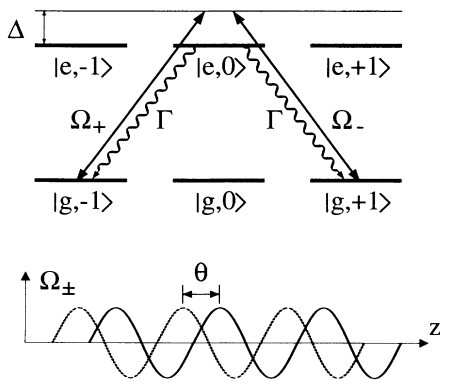

FIG. 1. Upper part: atomic-level scheme of a $J_g = 1$ to $J_e = 1$ transition in a $\sigma_\pm$ standing-wave configuration. Only the Λ system is physically relevant. Lower part: electric-field amplitudes of the $\sigma_\pm$ standing waves. Θ indicates the relative phase shift.

A proper theoretical description of cooling below the recoil limit requires a fully quantum-mechanical treatment of the center-of-mass motion of the atom. In the present paper we will solve the 1D master equation for laser cooling by quantum Monte Carlo methods, as outlined by us in detail in Refs. [10–12] (see also the related papers [13]). Furthermore, we will calculate the energy spectrum of the optical potentials in the limit of weak excitation to identify the dark state and "almost" dark states in the band structure. This band structure calculation is the basis for a rate equation analysis [14] which is valid in the limit of sufficiently large detunings. We emphasize that in contrast to the RW case there are *no* closed families of states as in the SW configuration to simplify the calculations.

The topics to be addressed in this paper are the kinetic energy $E = \langle p^2/2M \rangle$, the width of the momentum distribution, the dark-state population as a function of time, and the laser and atomic parameters for a given initial momentum distribution. We will also discuss our optimum parameters for polarization-gradient cooling and VSCPT and compare the SW and RW configurations. In Sec. II we summarize the basic equations for 1D laser cooling and establish our notation. In Sec. III we discuss the band structure and rate equation solution in the limit when the excited state is adiabatically eliminated. Finally, in Sec. IV we compare the RW and SW configurations. We find that for the SW a duty cycle which alternates between the optimum polarization gradient and VSCPT parameters gives significantly higher dark-state population than the RW.

II. BASIC EQUATIONS

A. Master equation

In this section we summarize the basic equations of laser cooling in one dimension and establish the notation for the following sections. We consider an atom with angular momentum J_g to J_e transition interacting with an electric field

$$\vec{E}(z,t) = \mathcal{E}\sum_\sigma \vec{e}^{\,*}_\sigma \epsilon_\sigma(\hat{z}) e^{-i\omega t} + \text{c.c.} \quad (8)$$

For the special case of two $\sigma_\pm$ standing waves the polarizations have a spatial dependence of $\epsilon_\pm(\hat{z}) = \cos(kz \pm \theta/2)$. In a rotating frame the atomic Hamiltonian for the atom interacting with the laser light is

$$H = \frac{p^2}{2m} - \Delta\sum_\sigma A^\dagger_\sigma A_\sigma - \frac{1}{2}\sum_\sigma [(-1)^\sigma \Omega^s_\sigma \epsilon_{-\sigma}(\hat{z}) A_\sigma + \text{H.c.}] \quad (9)$$

with $\Delta = \omega_L - \omega_{eg}$ the laser detuning, $\Omega = 2\mathcal{E}(e||D||g)/\sqrt{2J_e+1}$ Rabi frequencies, and

$$A_\sigma = \sum_{M_g,M_e} |J_g, M_g\rangle\langle J_g, M_g; 1, \sigma | Je, M_e\rangle\langle J_e, M_e| \quad (10)$$

atomic lowering operators given in terms of the Clebsch-Gordan coefficients. The terms on the right-hand side of Eq. (9) are the kinetic energy of the atom and the bare atomic and atom-laser interaction Hamiltonian, respectively.

The coupling of the atom to the vacuum modes of the radiation field leads to the master equation for the reduced atomic density operator,

$$\dot{\rho} = -i\left(H_{\rm eff}\rho - \rho H_{\rm eff}^\dagger\right) + \Gamma\sum_\sigma \int_{-k}^{+k} du N_\sigma(u)[A_\sigma(\hat{z})e^{-iu\hat{z}}]\,\rho[e^{+iu\hat{z}}A_\sigma^\dagger(\hat{z})]\,, \quad (11)$$

with

$$H_{\rm eff} = H - \frac{i}{2}\Gamma\sum_\sigma A_\sigma^\dagger A_\sigma \quad (12)$$

an effective (non-Hermitian) Wigner-Weisskopf Hamiltonian and Γ the spontaneous decay rate from the excited atomic state. The last term in the master equation describes the return of the atomic electron to the ground state when a spontaneous photon is emitted (including the associated momentum transfer to the atom). The light polarization of the emitted photon is $\sigma = 0, \pm 1$ and the corresponding angular distribution is given by $N_\sigma(u)$ while $\hbar u$ is the projection of the momentum of the spontaneously emitted photon along the z axis.

B. Adiabatic elimination of the excited state

For laser intensities far below saturation, $s = \frac{1}{2}\Omega^2/(\Delta^2+\Gamma^2/4) \ll 1$, the excited states of the atom can be eliminated adiabatically [15]. Making these approximations one can rewrite the master equation in terms of the reduced density operator involving only the atomic ground states,

$$\dot{\rho}_{gg} = -i\left(h_{\rm eff}\rho_{gg} - \rho_{gg}h_{\rm eff}^\dagger\right) + \gamma_0\sum_\sigma\int_{-k}^{+k} du N_\sigma(u)[B_\sigma(\hat{z})e^{-iu\hat{z}}] \times\rho_{gg}[e^{+iu\hat{z}}B_\sigma^\dagger(\hat{z})] \quad (13)$$

with the effective Hamiltonian

$$h_{\rm eff} = \frac{\hat{p}^2}{2M} + \left(U_0 - \frac{i}{2}\gamma_0\right)\sum_\sigma B_\sigma^\dagger(\hat{z})B_\sigma(\hat{z}) \quad (14)$$

$$\equiv \frac{\hat{p}^2}{2M} + V(\hat{z}) - \frac{i}{2}G(\hat{z})\,. \quad (15)$$

Note that the atomic lowering operators of Eq. (10) are replaced by Raman transition operators

$$B_\sigma(z) = \sum_{\sigma'}(-1)^\sigma A_\sigma A_{\sigma'}^\dagger \epsilon_{-\sigma'}^*(z), \quad (16)$$

which describe laser excitation according to the polarizations $\epsilon_\sigma(z)$ present at the position z and subsequent spontaneous decay back to the ground states. The effective Hamiltonian $h_{\rm eff}$ contains the ac Stark shift $U_0 = s\Delta/2$ and the optical pumping rate $\gamma_0 = s\Gamma/2$, which are both spatially modulated by $\sum_\sigma B_\sigma^\dagger(z)B_\sigma(z)$. The spatially modulated ac Stark shifts $V(z)$ act as potentials for the ground states and are called optical potentials.

C. Band structure and rate equations

For the Hermitian part of the effective Hamiltonian of Eq. (14) it is useful to define an eigenbasis. Looking at the optical potentials in Eq. (14) one finds that they have the translational symmetry $[T_{\lambda/2}, h_{\rm eff}] = 0$, where $T_{\lambda/2}$ is a translation operator $z \to z+\lambda/2$. Finding the common eigenvalues of these operators defines the band structure $E_n(q)$ and the Bloch eigenstates $|n, q\rangle = e^{-iq\hat{z}}|n, q\rangle$

$$H_q = \frac{(\hat{p}+q)^2}{2m} + V(\hat{z})\,, \quad (17)$$

$$H_q|n, q\rangle = E_n(q)|n, q\rangle\,, \quad (18)$$

$$T_{\lambda/2}|n, q\rangle = e^{iq\lambda/2}|n, q\rangle\,. \quad (19)$$

Here n is the band index and q is the quasimomentum, defined in the first Brillouin zone $q \in [-\hbar k, \hbar k]$. Note that $|n, q\rangle$ labels periodic wave functions defined and normalized in the unit cell $z \in [-\lambda/4, \lambda/4]$.

Using this Bloch eigenbasis, we can further simplify the master equation (13) by assuming that the coherences between different Bloch eigenstates are small (secular approximation) [14,12,16]. Neglecting the coherences between different bands $n \neq n'$ for a fixed q is valid if the energy separation between two Bloch states is much larger than the transition rate due to spontaneous emission, $|E_n(q) - E_m(q)| \gg \Gamma_n(q)$ $(\forall m, n, q)$. This is equivalent to $U_0 \gg \gamma_0$.

In this case the master equation reduces to a rate equation for the populations of the Bloch eigenstates, $\Pi_n(q) = \langle n, q|\rho_{gg}|n, q\rangle$, which reads

$$\frac{\partial}{\partial t}\Pi_n(q) = -\Gamma_n(q)\Pi_n(q) + \sum_m \int dq\, \gamma_{n,m}(q, q')\Pi_m(q'), \quad (20)$$

where the partial rates for transferring population from $\Pi_n(q)$ to $\Pi_m(q)$ are defined as

$$\gamma_{n,m}(q, q') = \gamma_0 \int_{-k}^{k} du \sum_\sigma N_\sigma(u)|\langle n, q|B_\sigma(\hat{z})e^{-iu\hat{z}}|m, q'\rangle|^2. \quad (21)$$

These partial rates add up to the total rate for depop-

ulating a Bloch state $\Gamma_n(q) = \sum_m \int dq' \ \gamma_{n,m}(q,q') = \gamma_0 \langle n,q\,|V(\hat{z})|n,q\,\rangle$. In Eq. (20) one sees that the optical pumping rate γ_0 is an overall factor on the right-hand side of the equation. This allows one to define a scaled time variable $\bar{t} = \gamma_0\, t$, which makes Eq. (20) independent of γ_0.

D. Quantum Monte Carlo wave function simulation

The parameter range for which one has to solve Eq. (11) determines the method to be used. Whenever it is possible we solve the rate equation Eq. (20), since the number of equations is significantly reduced. However, if the secular approximation cannot be made we have to solve either the full or the adiabatic eliminated master equation. This is done by using the method of quantum Monte Carlo simulation, which is described in detail in Refs. [12].

III. ADIABATIC ELIMINATION OF THE EXCITED STATE

A. Band structure

In this section we investigate laser cooling for the $J_g = 1$ to $J_e = 1$ transition for the laser configuration (4) under conditions where the excited state can be adiabatically eliminated. The Raman transition operators $B_\sigma(z)$ and the optical potentials $V(z)$ for the ground states $|g_{-1}\rangle$, $|g_{+1}\rangle$ are

$$B_-(z) = -\frac{1}{\sqrt{2}} \begin{pmatrix} 0 & 0 \\ \cos(\theta/2 + kz) & -\cos(\theta/2 - kz) \end{pmatrix}, \tag{22}$$

$$B_+(z) = \frac{1}{\sqrt{2}} \begin{pmatrix} \cos(\theta/2 + kz) & -\cos(\theta/2 - kz) \\ 0 & 0 \end{pmatrix}, \tag{23}$$

and

$$V(z) = \frac{1}{2} U_0 \begin{pmatrix} 2\cos^2(\theta/2 + kz) & -\cos(\theta) - \cos(2kz) \\ -\cos(\theta) - \cos(2kz) & 2\cos^2(\theta/2 - kz) \end{pmatrix}, \tag{24}$$

respectively. The state $|g_0\rangle$ does not enter our discussion since it is decoupled from the Λ system $|g_{-1}\rangle$, $|g_{+1}\rangle$.

Before discussing the band structure for the optical potential (24) it is worthwhile to recall the features of the potential and band structure in the familiar case of polarization gradient cooling in a J_g to $J_e = J_g + 1$ transition [14,12]. In this case by far the largest ac Stark shifts are found for the outermost $M = \pm J_g$ to $M = \pm J_e$ transitions. The *few lowest-energy eigenstates* in the optical potential are thus associated with the *diabatic* potential corresponding to these outer Zeeman levels. These low-lying eigenstates are an almost *flat* energy band as a function of the quasimomentum q [$E_n(q) \approx$const], i.e., tunneling to the neighboring wells is negligible. In contrast, in the present case the off-diagonal couplings in the optical potential (24) are of the same magnitude as the diagonal elements. These large off-diagonal elements are related to the existence of a dark state and result in a band structure that differs considerably from the one encountered in the $J_e = J_g + 1$ transition.

Figure 2 shows the band structure $E_n(q)$ as a function of the quasimomentum q for various potential depths U_0. To discuss these results, especially for low energies, it is convenient to introduce *adiabatic potentials*. These adiabatic potentials are obtained by diagonalizing the optical potential matrix $V(z)$ with the position variable z as a parameter. Labeling the two eigenstates by 0 and 1, we obtain the adiabatic potentials through Eq. (6). The existence of the flat potential $V^0_{ad}(z) = 0$ indicates that the system has a dark state. The first adiabatic eigenstate correspond to a superposition of the two ground states which decouples from the laser [$V^0_{ad}(z) = 0$] whereas the second couples to the excited state and has a nonzero optical potential $V^1_{ad}(z) \neq 0$ (Fig. 3). The motion in these two potentials is coupled by nonadiabatic effects.

For $\Delta > 0$ the ac Stark shift is positive and therefore the nonzero adiabatic potential is positive for all values of z which implies $V^1_{ad} > V^0_{ad}$. In the following we assume $\Delta > 0$ (or $U_0 > 0$), which is required to obtain polarization-gradient cooling. Thus we can distinguish three different zones in the band structure: (i) In the energy region $0 < E < \min[V^1_{ad}(z)]$ below the lower threshold of $V^1_{ad}(z)$ we find approximately the dispersion relation of a free particle corresponding to motion in $V^0_{ad}(z) = 0$. The two thresholds are indicated by dotted lines in Fig. 2. (ii) For intermediate energies

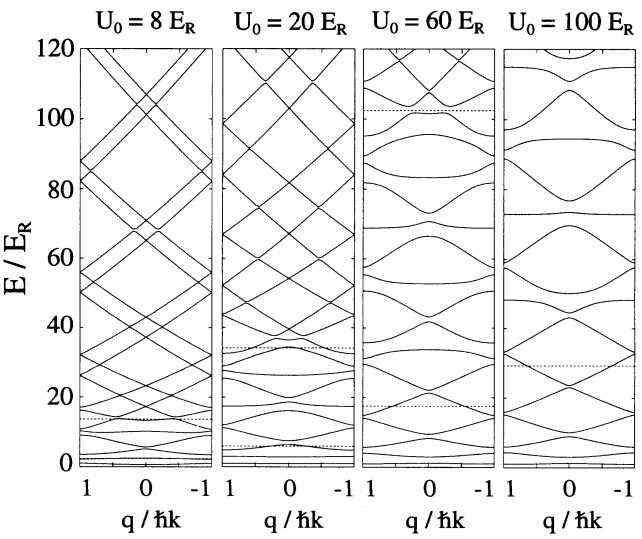

FIG. 2. Band structure in the optical potentials for a $J_g = 1$ to $J_e = 1$ transition interacting with two $\sigma_\pm$ standing waves with phase difference $\theta = \pi/4$. The dotted lines indicate the lower and upper thresholds of the nonzero adiabatic potential.

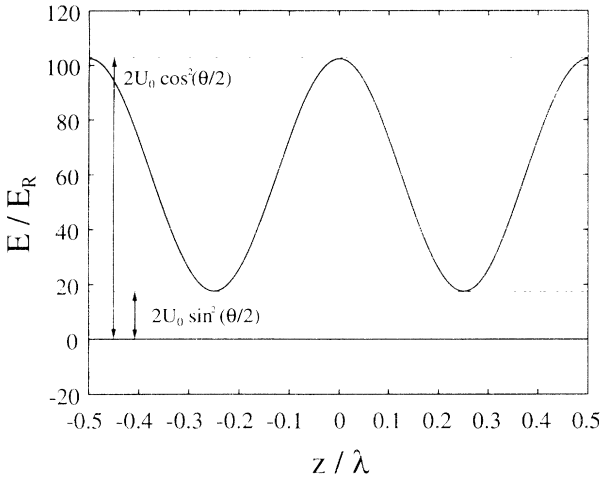

FIG. 3. Adiabatic potentials ($U_0 = -60$) for a $J_g = 1$ to $J_e = 1$ atom interacting with two $\sigma_\pm$ standing waves with phase difference $\theta = \pi/4$.

$\min[V^1_{ad}(z)] < E < \max[V^1_{ad}(z)]$ we have in addition a series of energy bands in $V^1_{ad}(z)$, although these states show strong nonadiabatic mixing with states in the potential $V^0_{ad}(z) = 0$. (iii) Finally, for energies above the upper threshold $E > \max[V^1_{ad}(z)]$, the adiabatic approximation breaks down. Using the basis $|g_{-1}\rangle \pm |g_{+1}\rangle$ separates the problem approximately for energies high above barrier. There the band structure behaves like two decoupled levels $E^{0,1}_n(q) = E^{0,1}_{thres} + (q + n\hbar k)^2/2m$, with different thresholds $E^{thres}_0 = U_0 \cos^2(\theta/2)$ and $E^{thres}_1 = U_0 \sin^2(\theta/2)$.

The dark state (5) is an eigenstate of the Hamiltonian (9) and we identify it in the band structure with the state $q = -\hbar k$ in the first band. The dark state has no potential energy and zero damping since the ac Stark shift and the optical pumping rate in Eq. (13) have the same spatial dependence.

In the rate equations the decay rate (loss rate due to optical pumping) of the dark state $\Gamma_{n=1}(q = \pm 1)$ in Eq. (20) is zero. In addition to this dark state one finds states that have a very small decay rate ("almost" dark states). In contrast to the σ_+, σ_- running-wave case, where states with small decay rates always were members of a momentum family $\mathcal{F}(p)$ with $p \approx 0$, these almost dark states for the lin $\angle$ lin configuration are located in higher bands. For example, the state with band index $n = 2$ and quasimomentum $q = 0$ has a very small decay rate. Looking at the momentum distribution of this state one finds that it consists predominantly of momentum components $0\hbar k$ and $\pm 2\hbar k$. The larger U_0 is, the smaller this decay rate. This is consistent with the fact that for larger U_0 the adiabatic approximation becomes more accurate. In the adiabatic approximation all states in the potential $V^0_{ad}(z)$ state are dark.

Comparing the decay rates of various Bloch states one finds that states with higher energies decay faster than the ones at lower energy. This is an indication for polarization-gradient cooling. We will give a qualitative picture for the process of polarization-gradient cooling in this configuration in Sec. V.

B. Solution of the rate equations

In this subsection we discuss numerical results obtained by solving the master equation (11) in a parameter range where the rate equation (20) is valid. We note that the rate equation depends only on the dimensionless time variable $\gamma_0 t$ and the parameter U_0/E_R. We will see in Sec. IV below that the rate equation limit is not necessarily the optimum parameter range for polarization-gradient-assisted dark-state cooling.

Figure 4 shows the time evolution of the momentum distribution $\rho(p,p)$ for different interaction times. This result was obtained by integrating the rate equations (20) with 50 bands and discretizing the quasimomenta on a grid $\Delta q = \hbar k/10$. For the initial condition we took a distribution of equally populated bands with energy $E \leq 250E_R$, which corresponds approximately to a flat momentum distribution of width $\pm 16\hbar k$. We see that the initially broad momentum distribution is rapidly compressed to a narrow Gaussian distribution. This corresponds to polarization-gradient cooling. Somewhat surprisingly, the width of this Gaussian distribution is narrower than one obtained for the familiar polarization gradient cooling on a $J_c = J_g + 1$ transition. For example, in Fig. 4 the width of the distribution at $\gamma_0 t = 60$ is $2.5\hbar k$, which is equivalent to a kinetic energy of $6.25E_R$. This has to be compared with the minimum energy of $40E_R$ for the $1/2 - 3/2$ transition [14,12]. For longer interaction $\gamma_0 t \approx 300 - 500$ the dark state and the almost dark states are populated and subrecoil peaks at $\pm 2\hbar k, \pm 1\hbar k$, and $0\hbar k$ appear. For long interaction times only states near the dark state are significantly populated. From Fig. 4 one can see very clearly that polarization-gradient cooling and dark-state cooling occur on entirely different time scales. The momentum distribution becomes a quasistationary Gaussian distribution on a time scale of the

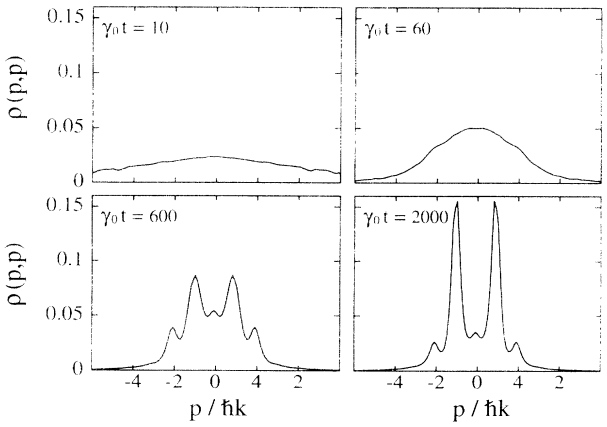

FIG. 4. Momentum distribution $\rho(p,p)$ for different interaction times, calculated by solving the master equation in the secular approximation. The rate equation was solved including 50 bands and 20 quasimomenta per band. As the initial condition equally populated bands with an energy smaller than $250E_R$ were assumed. The value for U_0 is $40E_R$. The width of the the momentum distribution for $\gamma_0 t = 60$ (quasisteady state for polarization gradient cooling) is $2.5\hbar k$ ($\langle E_{\rm kin}\rangle = 6.25E_R$).

order of $10/\gamma_0$ while the population of the dark occurs at a significantly lower rate.

In Fig. 5 we plot the expectation value of the total energy E as a function of the potential depth U_0 (in units of E_R) for different times. For short interaction times we find the qualitative behavior expected for polarization gradient cooling, namely, the existence of a minimum of the energy for $U_0 = 70E_R$ ($\gamma_0 t = 60$). For shallow potential depths the momentum distribution develops a broad background with high momentum tails which tend to increase the energy expectation value. On the other hand, a very deep potential depth leads to a strong localization of the atoms which decreases the cooling rate (Lamb-Dicke narrowing) [12].

For longer interaction times lowest energies are found in Fig. 5 for smaller values of U_0. The reason for this behavior is that the larger the potential depth, the slower the optical pumping time into the dark state. To illustrate this, we plot the pumping rate into the dark state as a function of the potential depth in Fig. 6. As pointed out before the time scales of the two cooling processes are clearly distinguishable, as shown in the inset of Fig. 6, where the energy expectation value is plotted as a function of time. After the polarization-gradient cooling has reached its quasistationary state the energy decays exponentially $\propto \exp(-\gamma_{\mathrm{VSCPT}} t)$. In Fig. 6 we plot this rate as a function of U_0. According to this figure this rate is three orders of magnitude smaller than γ_0 and decreases with increasing potential depth. This can be explained by studying the partial rates into the dark states $\gamma_{1,n'}(q = -\hbar k, q')$. One finds that the rates peak at energies $E_n(q)$, which are close to the upper threshold of V^1_{ad}. This is expected since the overlap integral in Eq. (21) is maximized when the wave function $|n', q'\rangle$ oscillates in space with the same wave number as the dark state $|D\rangle$. The spatial dependence of the dark state is that of a momentum eigenstate with momentum $\pm\hbar k$, which therefore has the maximal overlap with wave functions

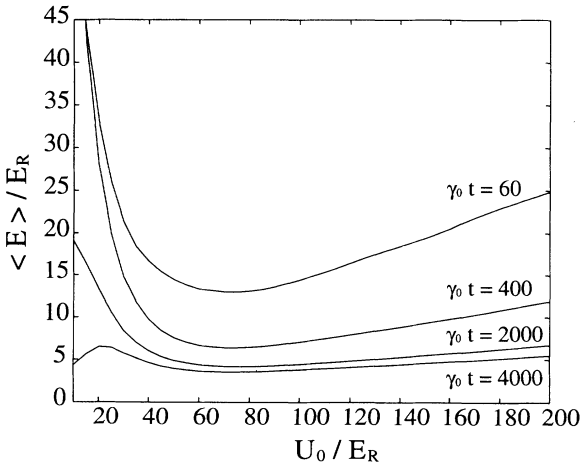

FIG. 5. Expectation value of the total energy $E = \langle \hat{p}^2 \rangle / 2m$ as a function of the potential depth U_0/E_R for various interaction times. For short interaction times one finds a minimum for the energy at $U_0 = 60E_R$. This minimum is shifted to smaller values for longer interaction times due to VSCPT.

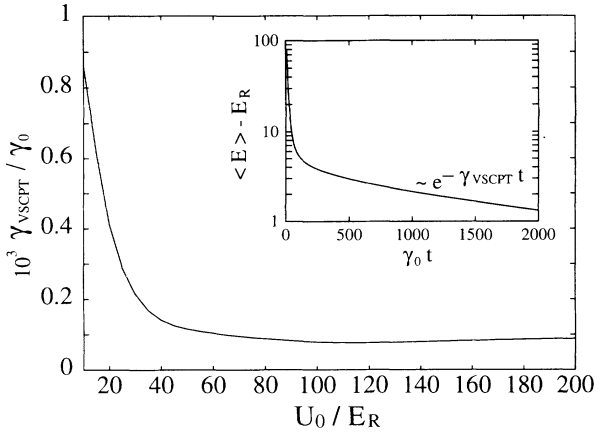

FIG. 6. VSCPT cooling rate γ_{VSCPT} as a function of potential depth U_0/E_R. The VSCPT cooling rate is three orders of magnitude smaller than the cooling rate for polarization gradient cooling. Smaller potential depths improve the VSCPT cooling rate.

whose energy are slightly above threshold. Polarization-gradient cooling tends to localize the atom near the bottom of the potential V^1_{ad}. Since for large potential depths only the few lowest eigenstates in V^1_{ad} are populated, the pumping rate into the dark state decreases with U_0.

IV. COOLING EFFICIENCY, OPTIMUM PARAMETERS, AND COMPARISON BETWEEN SW AND RW CONFIGURATIONS

In this section we discuss the efficiency of polarization-gradient-assisted VSCPT and give a comparison between the SW and RW cases. The basis of our discussion is provided by numerical results from quantum Monte Carlo simulations without adiabatic elimination of the excited state.

The question of optimum cooling parameters and the comparison of the RW and SW configurations depends on the physical observable that is considered and on the specific atom studied. The momentum distributions found in VSCPT are (non-Gaussian) distributions with two sharp peaks near $\pm\hbar k$ on top of a broader background. Observables of interest describing these narrow features are the "population" of dark state and the corresponding widths of the momentum distribution. The total kinetic energy $E = \langle \hat{p}^2 \rangle / 2m$, on the other hand, is a "global" feature of the distribution and in the present case is often dominated by the broad background [17].

For RW VSCPT we define in the following the dark-state population Π_{dark} as

$$\Pi_{dark}(\Delta q) = \int_{-\Delta q/2}^{\Delta q/2} dp \langle \Psi_{NC}(p) | \rho | \Psi_{NC}(p) \rangle \qquad (25)$$

with $|\Psi_{NC}(p)\rangle$ noncoupled states given in Eq. (2) [3]. The dark state has zero measure and therefore we integrate over a small interval which in the following is taken as $\Delta q = \hbar k/4$. If this interval is small $\Delta q \ll \hbar k$ the

dark-state population is directly related to the heights of the two peaks at $p = \pm\hbar k$ in the momentum distribution. In the same manner, we define the dark-state population for the SW case by replacing the momentum family with the Bloch eigenstates $|n, q\rangle$ in the first energy band,

$$\Pi_{dark}(\Delta q) = \int_{-\Delta q/2}^{\Delta q/2} dp' \langle n = 1, q - \hbar k \,|\rho| n = 1, q - \hbar k \rangle. \tag{26}$$

Another important quantity is the full width at half maximum (FWHM) (Δp_{dark}) of the two peaks at $p = \pm\hbar k$. The inverse of this width $\Delta x_{dark} = \hbar/\Delta p_{dark}$ is an approximate measure for the spatial coherence of the density matrix $\rho(x, x')$. If Δp_{dark} goes to zero, the atom is in a pure state and the spatial coherence is therefore infinitely extended.

When comparing these quantities we will distinguish between light ($\Gamma > \omega_R$) and heavy ($\Gamma \gg \omega_R$) atoms. For the case of light atoms we choose helium on the $2s\,^3S_1 \rightarrow 2p\,^3P_1$ transition. The atomic parameters are $\Gamma = 1.6$ MHz and $\omega_R = 42.5$ kHz so that $\Gamma = 37.5\omega_R$. A time step of $\omega_R t = 1$ corresponds to $t = 23.5$ μs. The width (FWHM) of the momentum distribution after Doppler cooling is $\Delta p = 6.1\hbar k$. We have also performed calculations for sodium, representing a heavy atom. For sodium on the $^3S_{1/2}, F_g = 1 \rightarrow {}^3P_{1/2}, F_e = 1$ transitions the atomic parameters are $\Gamma = 10$ MHz and $\omega_R = 25$ kHz ($\Gamma = 400E_R$). The width of the Doppler distribution is $\Delta p = 20\hbar k$. We note that in contrast to Na, polarization-gradient cooling for He gives temperatures not much different from Doppler cooling. The parameters in our model are the Rabi frequency Ω, the laser detuning Δ, the interaction time t, and the width of the initial distribution.

A. Optimum parameters for the RW configuration

In order to have a fair comparison we first investigate the optimum conditions for the standard $\sigma_\pm$ RW VSCPT [3]. For a given atom the quantities one can vary are the Rabi frequency Ω and the laser detuning Δ. Our goal is to maximize the dark-state population for a certain interaction time starting from an initially broad momentum distribution (Doppler cooling). We will see below that for VSCPT in a RW configuration there exists an optimum Rabi frequency. The optimum detuning is $\Delta = 0$ (on resonance).

The optimum Rabi frequency is determined by the following considerations: (i) The excitation profile of the laser light should excite as many atoms as possible in the given initial velocity distribution (capture range). Increasing the Rabi frequency will power broaden the atomic transition and thus increase this velocity range. This range determines the number of atoms that are eventually pumped into the dark state; atoms outside this excitation profile will be lost. (ii) VSCPT is based on a random walk between momentum families and scattering more photons in a given time will increase the number of "trials" to fall into the dark state. From this perspective, it is preferable to work at large values of the Rabi frequency (saturation) to increase the scattering rate. (iii) If the Rabi frequency is too large, the process of the coupling of the noncoupled state $|\psi_{NC}(p)\rangle$ back to the coupled ground state $|\psi_C(p)\rangle$ loses its velocity selectivity. According to Ref. [3], for low Rabi frequencies the velocity selective decay rate $|\psi_{\rm NC}(p)\rangle \rightarrow |\psi_C(p)\rangle$ scales as $\Gamma'' \approx \Gamma(kp/m)^2/\Omega^2$ and states with a family index $|\,p\,| \neq 0$ have a very long lifetime and are "practically dark."

In Fig. 7 we plot the decay rate of the dark state as a function of the atomic velocity for different Rabi frequencies. The decay rate was obtained by diagonalizing the effective Hamiltonian $H_{\rm eff}$ in a given family $\mathcal{F}(p)$ and plotting twice the imaginary part of the smallest eigenvalue. As expected, for the family index $p = 0$ the decay rate is exactly zero and for a small region around the dark state the decay rate is very small (Raman hole). With increasing Rabi frequency the Raman hole gets deeper and broader. To explain this we recall that the reason for the Raman hole is a destructive interference between the σ_+ and σ_- transition. This destructive interference is complete for zero Raman detuning. Only the momentum family with family index $p = 0$ leads to zero Raman detuning, in contrast to the Doppler shifted momentum families with $p \neq 0$. If the Rabi frequency is much larger than this Doppler-induced Raman detuning, the difference in transition amplitudes for the $\sigma_\pm$ transition is small and the cancelation therefore almost complete. For He the Raman hole is much narrower than for Na (Fig. 7). The reason is the different spontaneous decay widths; in addition, for a given momentum p the Doppler shift for Na is much smaller than for He. As a consequence, the capture range of Na is much larger than for He, but unfortunately the Raman hole for Na is also broader.

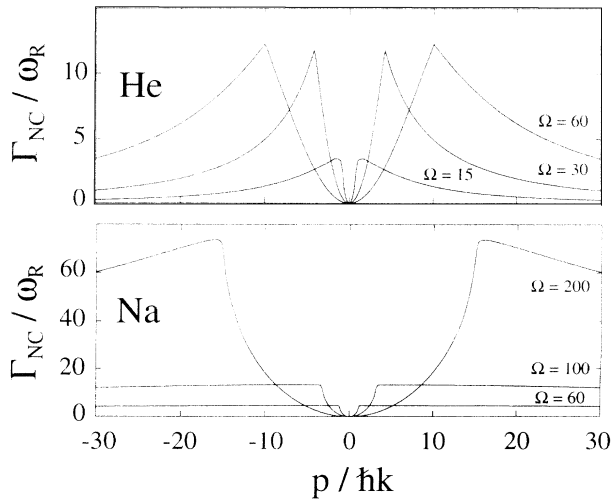

FIG. 7. Decay rate of the (nonperturbative) noncoupling state $|\psi_{NC}\rangle$ as function of the family index p, for the case of helium atoms ($\Gamma = 37.5\omega_R$) and sodium atoms ($\Gamma = 400\omega_R$). For $p = 0$ the decay rate vanishes. The width (FWHM) of the Raman hole is approximately $\Omega/2$.

The optimum value for the laser detuning is $\Delta = 0$. This is easily understood by applying the arguments above. If the transition is not driven on resonance, the Rabi frequency has to be increased in order to obtain the same number of scattered photons as for zero detuning. Increasing the Rabi frequency broadens the Raman hole and therefore makes the VSCPT less efficient.

In Fig. 8 we plot the dark-state population as a function of Rabi frequency for the case of Doppler cooled He and Na atoms. The optimum value for the Rabi frequency for He is $\Omega \approx 20\omega_R = 0.53\Gamma$ for a short interaction time ($\omega_R t \approx 30$). This corresponds to a saturation parameter $s = 0.56$. For longer interaction times the optimum Rabi frequency is shifted to larger values ($\Omega \approx 30\omega_R$ for $\omega_R t \approx 300$) since a larger capture range is required to excite atoms which have diffused to larger momenta. For an initial distribution which is broader than the Doppler cooling distribution for He, the optimum Rabi frequency is shifted to larger values, e.g., $\Omega = 40\omega_R$ for an initial momentum width $\Delta p = 8\hbar k$. For Na the spontaneous decay width is much larger than the recoil energy and our conclusions regarding the optimum Rabi frequency change correspondingly. In contrast to He, which could be driven close to saturation without losing velocity selectivity, for a given momentum p the Doppler shift for Na is much smaller (relative to Γ). From Fig. 8 we see that the optimum Rabi frequency for Na is $\Omega = 70\omega_R$ for a short laser interaction and $\Omega = 100\omega_R$ for the long time regime; these values correspond to a saturation parameter of $s = 0.06$ and $s = 0.125$, respectively. Comparing the numbers of photons scattered in a time interval $1/\omega_R$ for He and Na one finds that these numbers are approximately the same $(s_{\rm opt}\Gamma/\omega_R)_{\rm He} \approx (s_{\rm opt}\Gamma/\omega_R)_{\rm Na}$, with $s_{\rm opt}(< 1)$ the optimum saturation parameter. Very similar conclusions are derived for VSCPT in a SW configuration with the laser tuned on resonance, i.e., when there is no polarization-gradient cooling.

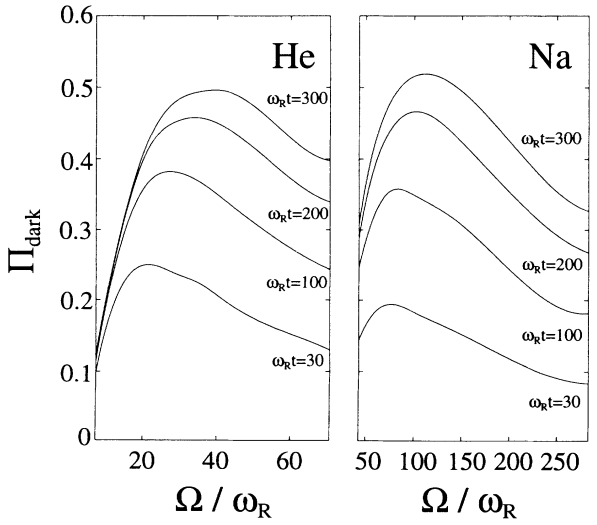

FIG. 8. Dark-state population as function of Rabi frequency for the case of RW VSCPT for helium and sodium.

B. Optimum parameters for the SW configuration and comparison of RW vs SW

The results of our comparison between the SW and RW configuration are summarized in Figs. 9–11 (for He) and Fig. 12 (for Na). These figures illustrate the time evolution of the dark-state population (Figs. 9 and 12), the width of the momentum distribution Δp (Fig. 10), and the kinetic energy E (Fig. 11). The initial momentum distribution in these plots corresponds to Doppler cooling.

Before discussing these figures in detail we find it worthwhile to make the following remarks.

(i) Polarization-gradient cooling gives the lowest temperatures for low intensities and large detunings [14]. VSCPT, on the other hand, works best on resonance. Thus polarization-gradient cooling and VSCPT have their optimum values in quite different regions of parameter space. The question of finding optimum detuning and Rabi frequency must always involve a trade-off between polarization gradient and VSCPT. This motivates us to study two scenarios: (a) The laser Rabi frequency and laser detuning are kept constant as a function of time; the optimum parameters for the RW and SW are determined by optimizing the dark-state population for a certain interaction time. (b) We study a duty cycle for the SW configuration where we alternate in time between the optimum Rabi frequency and detuning for VSCPT and polarization-gradient cooling.

(ii) The discussion below will identify the role of polarization-gradient cooling in combination with VSCPT as twofold: First, polarization-gradient cooling provides a *precooling* of the initial distribution, and second, *confinement* of the momentum distribution to a region of a few $\hbar k$ (suppression of atomic escape). The first effect is the dominant mechanism for short interaction times (as in atomic beam experiments). The relevance of precooling depends strongly on the width of the initial momentum distribution: for Doppler cooled He, for example, there is no need to precool, while for Doppler cooled Na precooling is essential. On the other hand, confinement of the velocity distribution by polarization-gradient cooling and the coexistence of this cooling mechanism with VSCPT is essential for the long time behavior.

In Fig. 9 we plot the dark-state population as a function of time for He. The solid line was calculated for the case of standard VSCPT of helium with counterpropagating $\sigma_\pm$ waves. The parameters $\Omega = 30\omega_R$ and $\Delta = 0$ correspond to the optimum value for this configuration (for a time $\omega_R t = 600$). This has to be compared with the dash-dotted line, which shows the time dependence of the dark-state population for the SW cooling scheme ($\Omega = 150\omega_R$ and $\Delta = 150\omega_R$). As mentioned above, for short interaction times the case of $\Delta = 0$ shows the most dark-state population, but after an interaction time of ($\omega_R t \approx 300$) the two curves cross and the SW scheme becomes more efficient. For these times one is in the regime where most of the population, which was originally located around $p \approx 0$, is either trapped in the dark state or has been heated up to large momenta. If no

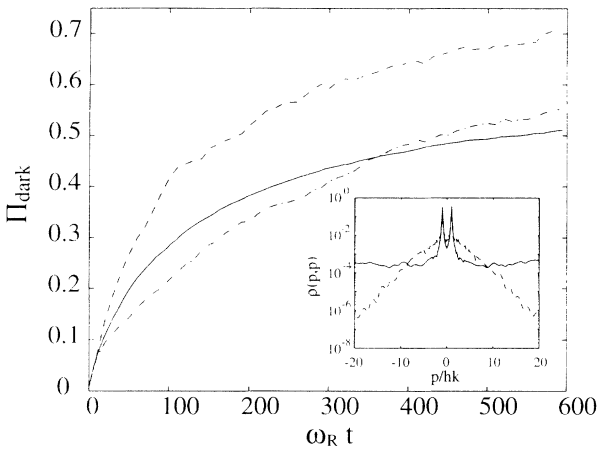

FIG. 9. Dark-state population as function of interaction time for the case of helium atoms ($\Gamma = 37.5\omega_R$). Solid line, $\sigma_\pm$ running-wave laser configuration with $\Delta = 0$ and $\Omega = 35\omega_R$; dash-dotted line, $\sigma_\pm$ standing-wave laser configuration ($\theta = \pi/4$) with $\Delta = 150\omega_R$ and $\Omega = 150\omega_R$; dashed line, $\sigma_\pm$ standing-wave laser configuration ($\theta = \pi/4$) with time-dependent laser parameters (duty cycle). Ω varies from $15\omega_R$ to $170\omega_R$. Δ varies from $0\omega_R$ to $190\omega_R$. The inset shows a logarithmic plot of the momentum distribution at $\omega_R t = 600$. For the RW (solid line) the distribution has significantly broader wings than for the SW with duty cycle (dashed line). This illustrates the compression of the momentum distribution by polarization gradient cooling.

polarization-gradient cooling is present, the rate of populating the dark states becomes small since atoms with large momenta need to scatter many photons in order to become trapped in the dark state. This causes the dark-state population to saturate in time. Polarization-gradient cooling keeps the momentum distribution confined and the saturation of the dark-state population as a function of time happens at later times (see the inset in Fig. 9). The width of the momentum distribution as a function of time is plotted in Fig. 10. We note that

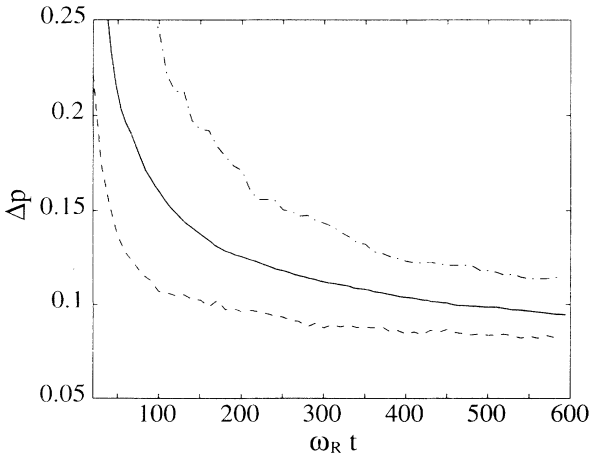

FIG. 10. Width of the peaks at $p = \pm\hbar k$ as function of the interaction time. Solid line, RW VSCPT; dash-dotted line, SW VSCPT; dashed line, SW VSCPT with duty cycle. For parameters see Fig. 9.

for the SW configuration (dash-dotted line) we find a broader width than for the RW (solid line) since for the SW the large Rabi frequency leads to a broader Raman hole.

One might expect a more pronounced improvement when using the polarization-gradient-assisted VSCPT. However, the polarization-gradient-cooling mechanism, which keeps the momentum distribution confined, makes the VSCPT less efficient so that in sum the improvement is not so significant. A solution to this problem is to alternate the laser parameters between the regime where either polarization-gradient cooling or VSCPT works at its optimum values. This *duty cycle* combines the advantages of both mechanisms. During a cycle with large detuning, polarization-gradient cooling compresses the momentum distribution and cools those atoms which were heated during a VSCPT cycle. This is followed by a cycle with $\Delta = 0$, which pumps the population within the VSCPT capture range in the dark state. We emphasize that the coexistence of polarization-gradient cooling and VSCPT is crucial for such a duty cycle since during the period of polarization-gradient cooling the population in the dark-state is preserved.

Figure 11 illustrates this duty cycle, where the dark-state population and the total energy of the atom are shown as a function of time. The dotted lines indicate times when the laser parameters are switched from $\Omega = 180$ and $\Delta = 200$ for the polarization gradient cycle to $\Omega = 10$ and $\Delta = 0$ in units of E_R for the VSCPT cycle. For the duration of the cycle we took $\omega_R T_{\text{cycle}} = 5$, which corresponds to an interaction time where polarization-gradient cooling is almost stationary. As modulation, a smoothed square function was assumed so the transition between the two sets of parameters was not abrupt. From Fig. 11 we see that whenever the laser parameters are set for optimum polarization-gradient cooling, the en-

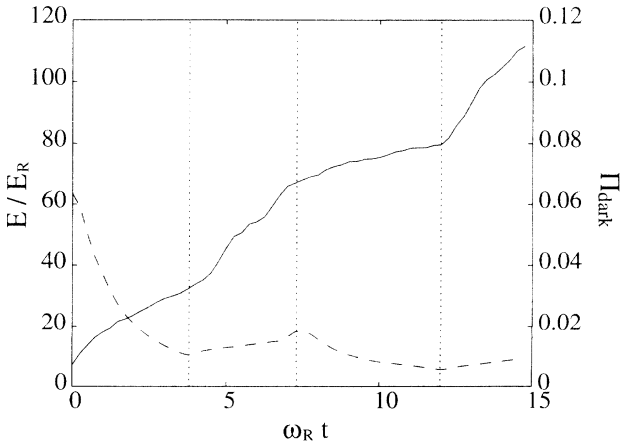

FIG. 11. Dark-state population (solid line) and energy expectation value (dashed line) as function of time for time-dependent laser parameters. For the first and the third time period (dotted lines) $\Omega = 180$ and $\Delta = 200$ (optimum polarization-gradient cooling). For the second and the fourth time period $\Omega = 10$ and $\Delta = 0$ (optimum VSCPT) in units of E_R.

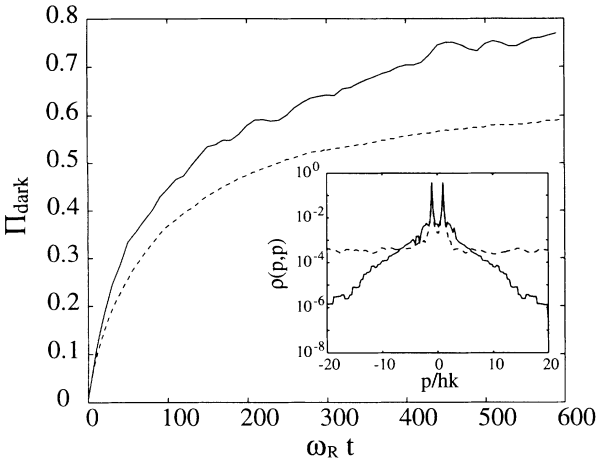

FIG. 12. Dark-state population as function of interaction time for the case of sodium atoms ($\Gamma = 400\omega_R$). Solid line, $\sigma_\pm$ running-wave laser configuration with $\Delta = 0$ and $\Omega = \omega_R$; dashed line, $\sigma_\pm$ standing-wave laser configuration ($\theta = \pi/4$) with time-dependent laser parameters (duty cycle): $\Omega = 200$ and $\Delta = 150$ for the polarization-gradient cycle and $\Omega = 70$ and $\Delta = 0$ in units of E_R for the VSCPT cycle. The inset shows a logarithmic plot of the momentum distribution at $\omega_R t = 600$ (see Fig. 9).

ergy decreases, which corresponds to a compression of the momentum distribution. On the other hand, during the VSCPT cycle the energy increases, but the slope of the time-dependent dark-state population is much steeper. In Fig. 9 we compare this time-dependent scheme (dashed line) with the standard VSCPT (solid line). We see that for short interaction times as well as in the long time regime, alternating between polarization-gradient cooling a VSCPT improves the dark-state population significantly. In addition, in Fig. 10 the width of the peaks at $p = \pm\hbar k$ in the momentum distribution is narrower than that achieved with RW VSCPT (dashed line). The reason for the narrow peaks is that one can choose a relatively small Rabi frequencies during the VSCPT cycle since only a small capture range is required as the polarization-gradient-cooling cycle compresses the population around zero momentum. For the duty cycle we used a period of $\omega_R T_{\text{cycle}} = 4$, which is shorter than the time required to reach the quasistationary state for polarization-gradient cooling but leads to an improvement in the short time regime, since already for $\omega_R t = 8$ a full VSCPT cycle is performed.

Finally, Fig. 12 compares the different cooling schemes for the case of Na. As mentioned above, for Na a small saturation parameter ($s \approx 0.1$) leads to optimal RW VSCPT. For a small saturation parameter the results for Na are very similar to those obtained for He. Figure 12 shows that the SW scheme with time-dependent laser parameters (dashed line) improves the dark-state population for all interaction times.

V. CONCLUSION

In this paper we have presented a fully quantum-mechanical analysis of laser cooling on a $J_g = 1$ to $J_e = 1$ transition in a laser configuration consisting or two counterpropagating laser beams where the lasers are linearly polarized with angle $\theta = \pi/4$ between the polarization vectors. The essential feature of this configuration is the coexistence of subrecoil cooling (VSCPT) and polarization-gradient cooling. Polarization-gradient cooling occurs at a time scale significantly shorter than VSCPT. The optimum parameter values for polarization-gradient cooling and VSCPT are in a completely different parameter regime: Polarization-gradient cooling works best off resonance and for low intensities, while VSCPT works best on resonance.

The role of polarization-gradient cooling is twofold: First, for short interaction times it provides *precooling* of the initial momentum distribution to polarization-gradient temperatures (we find typically $\Delta p = 2.5\hbar k$ and we point out that these temperatures are considerably lower than what is expected for usual polarization-gradient cooling on a $J_e = Jg + 1$ transition). The relevance of precooling depends strongly on the width of the initial relative to the polarization gradient distribution. Second, in the long time limit polarization-gradient cooling leads to a *confinement* of the velocities to within a few $\hbar k$ *during* the phase of dark-state cooling. Thus polarization-gradient cooling compresses the high-energy tail of the velocity distribution. This eventually leads to a larger number of atoms being captured in the dark state (when compared with the scheme of Aspect *et al.* [3]).

We can combine the advantages of polarization-gradient cooling and VSCPT in a scheme where we cycle in time between the optimum cooling parameters for both cooling mechanism. This leads to an increased pumping time into the dark state and in the polarization-gradient cycle compresses the atoms that escape in VSCPT with $\sigma^\pm$ running waves.

In unpublished work we have generalized the above quantum calculations to 2D laser configurations. In addition we have performed quantum simulations for polarization-gradient-assisted dark-state cooling in a "flat bottom" trap (generated, for example, by far off-resonant laser light).

ACKNOWLEDGMENTS

The authors thank T. Bergeman and H. Metcalf and co-workers for comments and discussions. The work at JILA is supported in part by the National Science Foundation. The work at MIT is supported by Rome Laboratory Contract No. F19628-92-K-0013 and the work at Harvard University was supported by Office of Naval Research Grant No. ONR-N0014-91-J-1808.

[1] C. Cohen-Tannoudji and W.D. Phillips, Phys. Today **43** (10), 33 (1990); see contributions in *Proceedings LIKE Workshop*, edited by L. Moi (ETS Editrice, Pisa, 1991); and special issues on laser cooling, J. Opt. Soc. Am. B **6** (11) (1989); **2** (11) (1985).

[2] E. Arimondo, in *Laser Manipulation of Atoms and Ions*, Proceedings of the International School of Physics "Enrico Fermi," Course CXVIII, Varenna, 1991, edited by E. Arimondo, W. D. Phillips, and F. Strumia (North-Holland, Amsterdam, 1992), pp. 191–224.

[3] A. Aspect, E. Arimondo, R. Kaiser, N. Vansteenkiste, and C. Cohen-Tannoudji, Phys. Rev. Lett. **61**, 826 (1988); J. Opt. Soc. Am. B **6**, 2112 (1989).

[4] Experimental work for polarization-gradient-assisted dark-state cooling is in progress [H. Metcalf (private communication)].

[5] M. Kasevich and S. Chu, Phys. Rev. Lett. **69**, 1741 (1992).

[6] F. Mauri and E. Arimondo, Europhys. Lett. **16**, 717 (1991).

[7] M. A. Ol'shanii and V. G. Minogin, Quantum Opt. **3**, 317 (1991).

[8] C. Cohen-Tannoudji, F. Bardou, and A. Aspect, in *Laser Spectroscopy X*, edited by M. Ducloy, E. Giacobino, and G. Camy (World Scientific, Singapore, 1992).

[9] M.S. Shahriar, P.R. Hemmer, M.G. Prentiss, P. Marte, J. Mervis, D.P. Katz, N.P. Bigelow, and T. Cai, Phys. Rev. A **48**, R4035 (1993).

[10] M.S. Shahriar, P.R. Hemmer, M.G. Prentiss, A. Chu, D.P. Katz, and N.P. Bigelow, Opt. Commun. **103**, 453 (1993)

[11] R. Dum, P. Zoller, and H. Ritsch, Phys. Rev. A **45**, 4879 (1992); C. W. Gardiner, A. S. Parkins, and P. Zoller, *ibid.* **46**, 4363 (1992); R. Dum, A.S. Parkins, P. Zoller, and C.W. Gardiner, *ibid.* **46**, 4382 (1992).

[12] P. Marte, R. Dum, R. Taïeb, and P. Zoller, Phys. Rev. A **47**, 1378 (1993); Phys. Rev. Lett. **71**, 1335 (1993); R. Taïeb, P. Marte, R. Dum, and P. Zoller, Phys. Rev. A **47**, 1107 (1993); **47**, 4986 (1993).

[13] J. Dalibard, Y. Castin, and K. Mølmer, Phys. Rev. Lett. **68**, 580 (1992); K. Mølmer, Y. Castin, and J. Dalibard, J. Opt. Soc. Am. B **10**, 524 (1993); H. J. Carmichael (unpublished); N. Gisin and I.C. Percival, Phys. Rev. Lett. A **167**, 315 (1992).

[14] Y. Castin and J. Dalibard, Europhys. Lett. **14**, 761 (1991).

[15] We note the additional requirement that the detuning from resonance is assumed to be unchanged by the Doppler shift $\Delta \approx \Delta \gg p_{\max}\hbar k/2m$, where $p_{\max}$ is the largest momentum occurring in the problem.

[16] P. Marte (unpublished).

[17] In the case of a $\sigma_{\pm}$ RW configuration, for example, part of this background corresponds to atoms escaping to infinity: thus in the calculations one finds that, even though the dark-state population increases in time, the energy might also increase since it is dominated by the few escaping atoms.